Nanoscale Advances

ROYAL SOCIETY OF CHEMISTRY

PAPER

View Article Online
View Journal | View Issue

Cite this: *Nanoscale Adv.*, 2025, **7**, 4994

Synthesis of a hercynite supported phosphomolybdic acid magnetic nanocomposite as an efficient catalyst for the synthesis of N-heterocycles†

Kowsar Azizi,[a] Saba Ghasemi *[a] and Ahmad Nikseresht *[b]

Received 30th March 2025
Accepted 20th June 2025

DOI: 10.1039/d5na00295h

rsc.li/nanoscale-advances

In this study, a novel heteropoly acid (HPA) functionalized nanomagnetic catalytic composite was prepared by incorporating phosphomolybdic acid ($H_3PMo_{12}O_{40}$, PMA) into silica modified hercynite magnetic nanoparticles through a simple post-synthetic modification strategy. The obtained nanocomposite was thoroughly characterized using FT-IR, XRD, TGA-DSC, EDX, ICP-OES, elemental mapping, SEM, TEM, BET, and VSM analyses. The catalytic activity of the resulting heterogeneous catalyst was evaluated in the synthesis of 2,3-dihydroquinazolin-4(1*H*)-ones through the cyclocondensation of aldehyde or ketone compounds and anthranilamide under reflux conditions, achieving high yields in short reaction times. The key advantage of this catalyst lies in the combination of Brønsted acidity provided by the PMA and the Lewis acidity contributed by both the hercynite support and the PMA. Hot filtration and reusability tests demonstrated that the catalyst remains highly stable and can be reused multiple times without a significant loss in catalytic activity.

1. Introduction

2,3-Dihydroquinazolin-4(1*H*)-ones (DHQs) are an important class of nitrogen-rich aromatic heterocycles, characterized by a unique structural framework consisting of a benzene ring fused to a six-membered ring.[1,2] This structure incorporates two nitrogen atoms at positions 1 and 3, and a carbonyl group at position 4, with carbon-2 being the primary site of substitution within the chiral center of most DHQ derivatives. Due to this distinctive architecture, DHQs exhibit a wide range of applications across medicinal chemistry, materials science, biochemistry, and pharmacology.[1,3,4]

Among the various methods for DHQ synthesis, the direct cyclocondensation of anthranilamide with aldehydes is the most commonly used and convenient approach. Various catalysts, including bases, acids, iodine, and metal salts, have been explored for this reaction.[1,3,5–7] However, many of these catalysts face limitations due to their homogeneous nature or the complexity involved in synthesizing previously reported heterogeneous catalysts. These challenges necessitate the development of more efficient and sustainable catalytic systems for this important transformation.

Supported catalysts, in which an active catalytic phase is immobilized on a suitable support, offer several advantages, including enhanced stability, improved activity, and significantly improved ease of handling and separation.[8–12] Magnetic catalytic supports, in particular, provide substantial benefits such as facile separation from reaction mixtures using external magnetic fields. This enables efficient catalyst recovery and reuse, minimizing environmental impact and reducing production costs.[13–15]

Magnetic spinel oxides, composed of both transition and non-transition metals, exhibit diverse physicochemical properties and find applications in various fields, especially in organic synthesis. Their biocompatibility, small size, and superparamagnetic properties make them ideal candidates for catalytic support applications.[16] Among these, hercynite ($FeAl_2O_4$) nanoparticles, composed of iron and aluminum oxides, have garnered significant attention due to their potential for surface functionalization.[16–20] Hercynite possesses a cubic crystal structure with Fe occupying tetrahedral sites and Al occupying octahedral sites.[19] The presence of surface hydroxyl groups on hercynite provides avenues for further modification using surface modifiers such as SiO_2, enabling the introduction of specific functionalities for tailored catalytic applications.[21,22]

Heteropoly acids (HPAs) are versatile catalysts renowned for their strong acidity and catalytic activity in various reactions.[23,24] However, their homogeneous use is limited by difficulties in

[a]*Department of Chemistry, Il.C., Islamic Azad University, Ilam, Iran. E-mail: Sb.ghasemi@iau.ac.ir; Fax: +98-8433351849; Tel: +98-8432224827*

[b]*Department of Chemistry, Payame Noor University (PNU), P.O Box 19395-4697, Tehran, Iran. E-mail: a_nik55@yahoo.com; ahmad.nikseresht@pnu.ac.ir*

† Electronic supplementary information (ESI) available: Copies of the FT-IR, ^{1}HNMR, ^{13}CNMR, and mass spectra of some selected synthesized products. See DOI: https://doi.org/10.1039/d5na00295h

separation and recovery. Immobilization on solid supports, such as metal oxides or magnetic nanoparticles, addresses these challenges by enhancing catalyst stability, enabling easy separation, and improving sustainability and cost-effectiveness.[23–28]

To date, various Brønsted and Lewis acidic catalysts have been successfully grafted onto hercynite for diverse applications.[5,17,21,22,29–33] However, to the best of our knowledge, there have been no reports on the grafting of phosphomolybdic acid onto hercynite. In this study, phosphomolybdic acid is immobilized on a silica-modified hercynite support to create a novel nanomagnetic solid acid composite, which serves as a pioneering catalytic system for the synthesis of 2,3-dihydroquinazolin-4(1*H*)-ones.

2. Experimental

2.1. Materials and methods

All chemical reagents and solvents utilized in this study were acquired from Sigma-Aldrich in St. Louis, MO, USA, and Merck Chemical Co. in Darmstadt, Germany, without additional purification. The ^{1}H NMR (250 MHz) and ^{13}C NMR spectra (62.5 MHz) were acquired in dimethyl sulfoxide (DMSO-d_6) using a Bruker DRX-250 AVANCE spectrometer. All FT-IR spectra were recorded on a Bruker Vertex 70 spectrometer using KBr plates. The mass spectra were obtained using an Agilent G708 1B MSD instrument equipped with a Triple-Axis detector at 70 eV electron ionization. XRD analysis was conducted using a PHILIPS PW1730 (Netherlands) with a step size of 0.05° and Cu Kα radiation (1.54056 Å) at 40 kV and 30 mA. TGA analysis was performed using a TA Instruments Q600 (USA), employing Zero Air as carrier gas. EDX and EDX-Mapping analysis were performed using a TESCAN VEGA 3 SEM with a SAMX detector (France, Czech Republic). SEM analysis was performed using TESCAN MIRA II (Czech Republic). TEM analysis was conducted using a CM120 (Netherlands) with a maximum voltage of 100 kV. BET analysis was performed using a BEL BELSORP MINI II (Japan), with degassing provided by the BEL PREP VAC II (vacuum heating up to 450 °C). Magnetic property analysis was conducted using an MDKB instrument (Magnet Kavir Kashan Company), with a maximum applied field of 2 tesla and a dynamic range from 500 to 0.00005 emu.

2.2. Typical procedure for synthesis of Hercynite@SiO_2-PMA nanocomposite

Initially, Hercynite@SiO_2 MNPs were synthesized according to a previously reported method.[29] Subsequently, 1.5 g of the prepared Hercynite@SiO_2 was suspended in 100 mL of ethanol and sonicated for 30 min. Following this, 0.55 g of phosphomolybdic acid (0.3 mmol) was added to the suspension, and was sonicated for an additional 30 min. The mixture was then refluxed with vigorous stirring for 24 hours. Afterward, the solvent was evaporated, and the resulting powder was calcined at 550 °C for 5 hours. The obtained Hercynite@SiO_2-PMA nanocomposite was washed several times with hot water and ethanol, then dried at 120 °C for 24 hours.

2.3. General procedure for synthesis of 2,3-dihydroquinazolin-4(1*H*)-ones catalyzed by Hercynite@SiO_2-PMA magnetic nanocomposite

A mixture of an aldehyde or ketone (1 mmol), anthranilamide (1 mmol), Hercynite@SiO_2-PMA (20 mg), and 3 mL of deionized water was placed in a 15 mL round-bottom flask. The reaction was stirred under reflux conditions until completion, as monitored by TLC. Afterward, the reaction mixture was diluted with hot ethanol, and the magnetic catalyst was separated from the mixture. Although a neodymium magnet was employed to facilitate rapid and efficient separation, the catalyst could also be readily isolated using a standard magnet. Following separation, the catalyst was washed thoroughly with acetone and ethanol. The ethanolic solution was then cooled to room temperature, leading to the precipitation of the crude product. The precipitate was further purified by recrystallization from ethanol and dried to obtain the final product.

3. Results and discussion

In this research, a novel nanomagnetic HPA catalyst was synthesized through surface modification of hercynite nanoparticles with silica layers, followed by the immobilization of phosphomolybdic acid within their pores (Scheme 1). The structure of the prepared nanoparticles was comprehensively characterized by FT-IR, XRD, TGA, EDX, ICP-OES, EDX mapping, FE-SEM, TEM, BET, and VSM analyses.

3.1. Catalyst characterization

The FT-IR spectra for each stage of the catalyst synthesis process including hercynite, Hercynite@SiO_2, pure PMA, and Hercynite@SiO_2-PMA nanocomposite are shown in Fig. 1. In Fig. 1a, the absorption bands observed at 590 cm^{-1}, 871 cm^{-1}, and 3440 cm^{-1} correspond to the stretching vibrations of the Fe–O, Al–O, and O–H bonds, respectively. These peaks confirm the presence of hercynite in all the samples (Fig. 1b and d).[18] The SiO_2 coating on hercynite is evidenced by the strong peaks at 1090, 957, and 812 cm^{-1}, corresponding to the Si–O

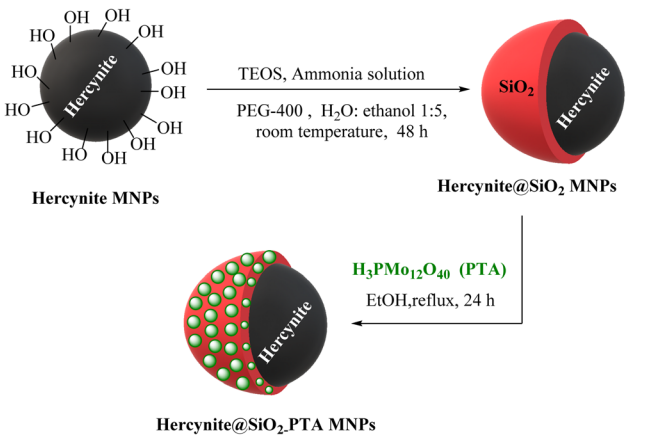

Scheme 1 Stepwise synthesis of Hercynite@SiO_2-PMA magnetic nanocomposite.

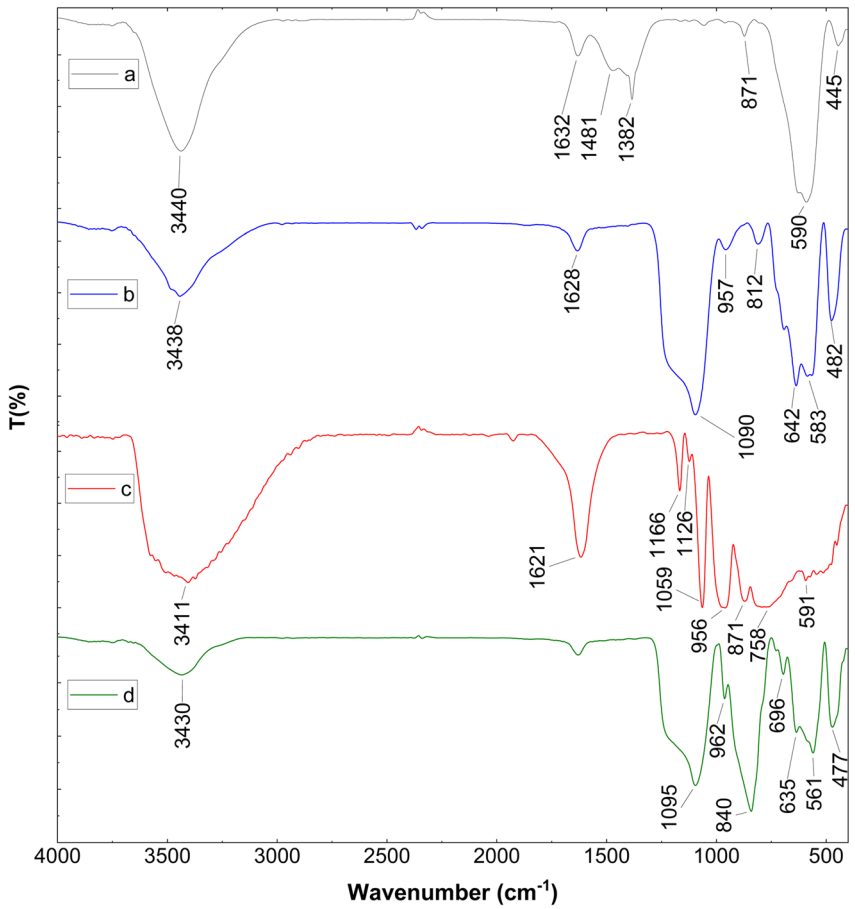

Fig. 1 FT-IR analysis of (a) hercynite, (b) Hercynite@SiO_2, and (c) pure PMA, (d) Hercynite@SiO_2-PMA.

bonds.[22,29] Additionally, the broad band observed at 3438 cm^{-1} is attributed to the stretching vibration of OH groups attached onto silica layer (Fig. 1b).[21] A comparison between pure PMA and the Hercynite@SiO_2-PMA sample reveals that some of the PMA peaks overlap with the Si–O bands in the Hercynite@SiO_2-PMA composite. However, after the addition of PMA, new

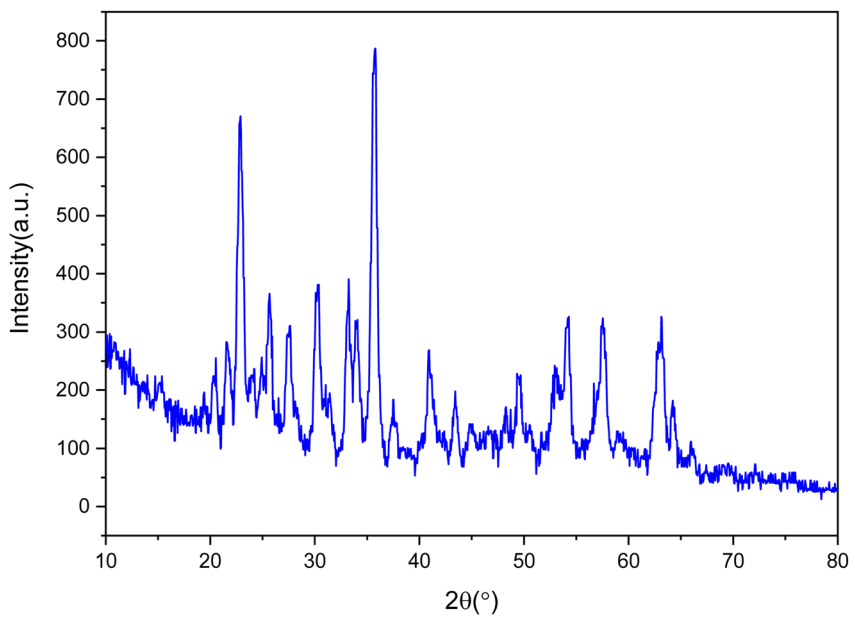

Fig. 2 XRD analysis of Hercynite@SiO_2-PMA.

absorption bands appear at 696, 840, and 962 cm^{-1}, which are characteristic of the PMA structure. The presence of these distinct additional peaks clearly confirms the successful synthesis of the targeted nanocomposite.

XRD analysis (Fig. 2) was employed to characterize the structure of the Hercynite@SiO_2-PMA. The sharp peaks observed at 2θ values of 30.28°, 35.73°, 43.43°, 54.18°, 57.53°, and 63.13° closely matched the characteristic peaks of hercynite reported in previous studies, confirming the preservation of the hercynite crystalline phase during the functionalization process.[34] Additional peaks at 2θ values of 20.53°, 21.53°, 22.83°, 25.68°, 27.63°, 33.23°, 34.08°, 37.48°, 40.88°, 44.78°, 48.28°, 49.33°, 64.23°, and 65.93° are attributed to the surface PMA, further supporting the successful formation of the targeted nanocomposite.[35,36]

Fig. 3 presents the results of thermogravimetric analysis coupled with differential scanning calorimetry (TGA-DSC) performed on Hercynite@SiO_2-PMA. The initial weight loss observed below 200 °C is attributed to the desorption of the adsorbed solvents and moisture. A subsequent weight loss occurring above 200 °C is likely due to the decomposition of the PMA groups grafted onto the surface of the magnetic nanoparticles.[37] This weight loss is further supported by an exothermic peak in the DSC curve, indicating an exothermic decomposition process. These findings collectively demonstrate the high thermal stability of Hercynite@SiO_2-PMA. This robust thermal behavior suggests that the material can withstand elevated temperatures. Therefore, it is suitable for applications in harsh reaction conditions, such as those encountered in catalytic processes or high-temperature environments.

The EDX analysis of Hercynite@SiO_2-PMA confirmed the presence of all expected elements. The detection of Fe, Al, and O originated from the magnetic hercynite core, while Si was observed from the surrounding amorphous silica shell. The presence of P and Mo within the spectrum indicated the successful incorporation of PMA groups (Fig. 4). Further quantitative analysis using ICP-OES revealed a P content of approximately 808.9 ppm and a Mo content of around 1169.6 ppm, confirming their successful incorporation into the support. Additionally, the ICP-OES analysis determined the contents of Fe and Al in the catalyst to be approximately 351 216.5 ppm and 4543.7 ppm, respectively.

Elemental mapping patterns of Hercynite@SiO_2-PMA reveal that Fe exhibits the highest density of distribution on the surface, likely originating from the hercynite core. In contrast, Al, O, and Si display a more homogeneous distribution, consistent with the presence of an amorphous silica shell. Notably, P and Mo elements demonstrate a uniform distribution across the surface, suggesting optimal accessibility for guest reactant species (Fig. 5).

SEM analysis of the Hercynite@SiO_2-PMA composite revealed a heterogeneous morphological landscape. The nanoparticle population exhibited a heterogeneous distribution, with particle shapes ranging from spherical and smooth to irregular and agglomerated (Fig. 6). These observations suggest a complex microstructure characterized by a coexistence of discrete nanoparticles and agglomerates.

TEM images of Hercynite@SiO_2-PMA reveal distinct core–shell nanoparticles. The core, composed of a dense and electron-rich hercynite component, is surrounded by a less

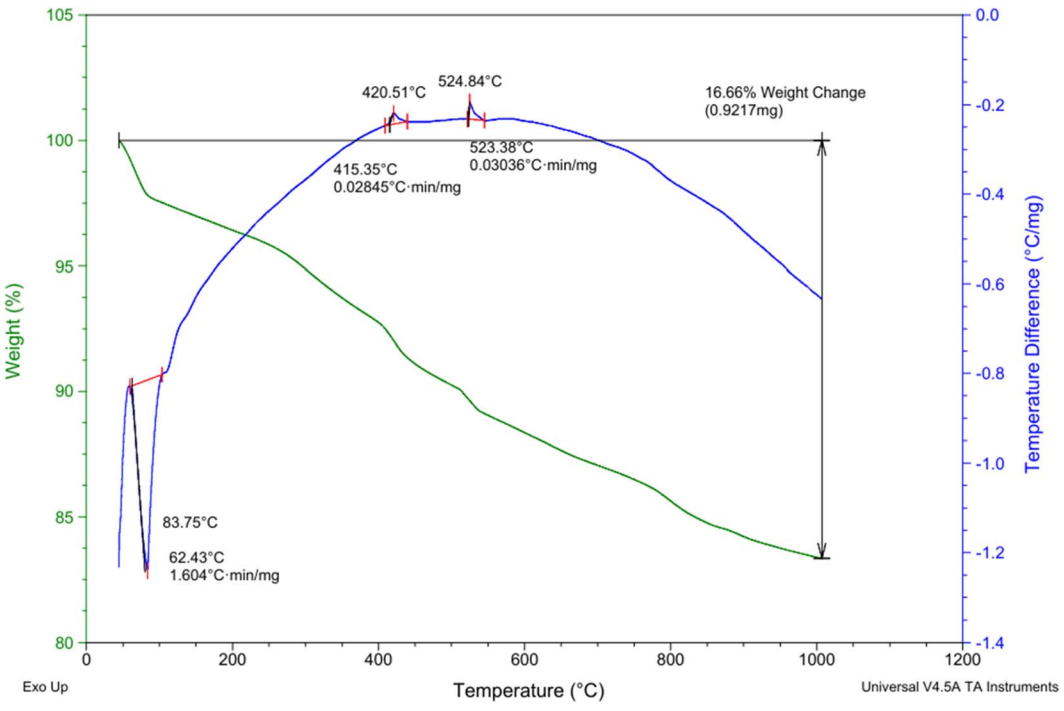

Fig. 3 TGA-DSC curves of Hercynite@SiO_2-PMA.

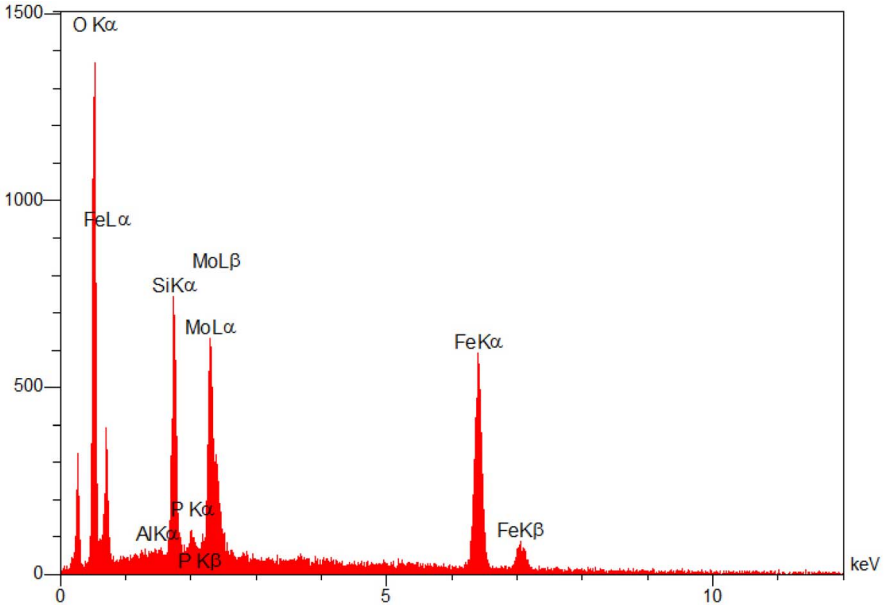

Fig. 4 EDAX analysis of Hercynite@SiO_2-PMA.

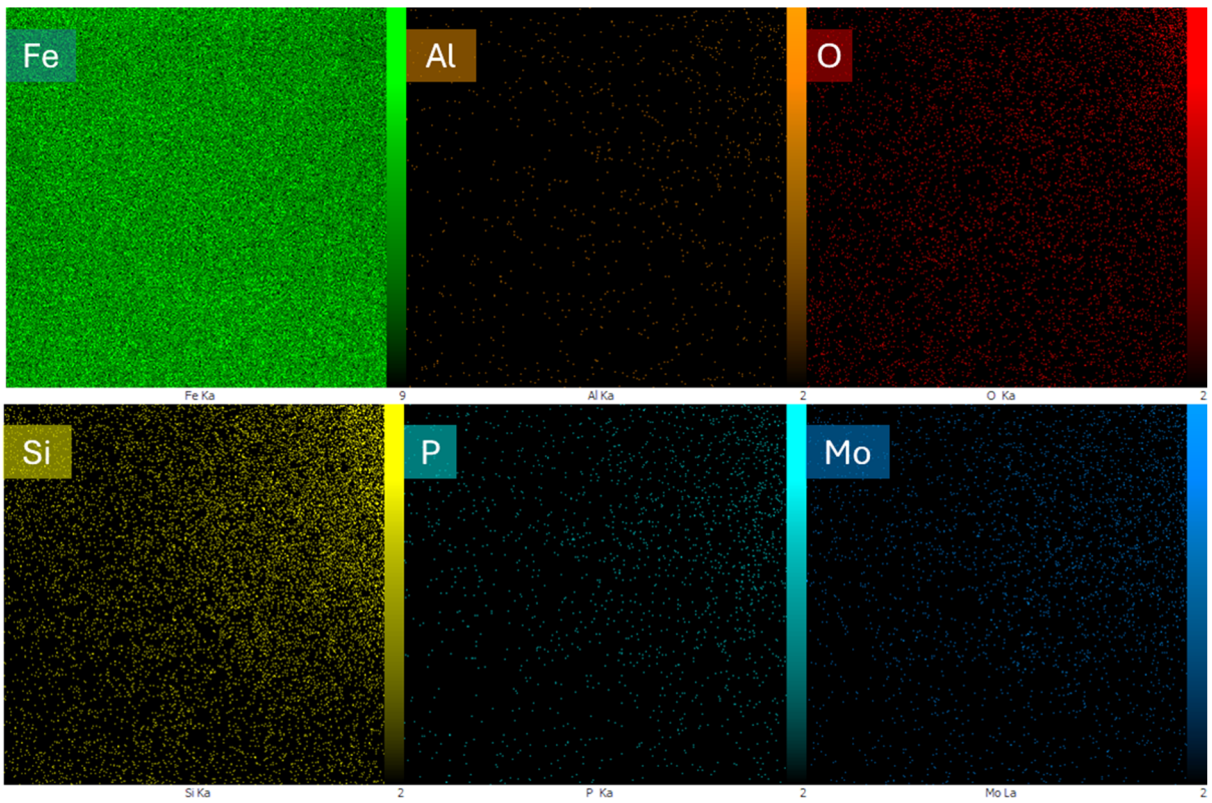

Fig. 5 Elemental mapping images of Hercynite@SiO_2-PMA.

dense, amorphous silica shell. Variations in particle size and the presence of agglomerates suggest a heterogeneous distribution and a complex microstructure (Fig. 7). These characteristics can significantly impact the material's properties and performance.

Fig. 8 illustrates the magnetic properties of Hercynite@SiO_2-PMA as measured by vibrating sample magnetometry (VSM). The material exhibits a saturation magnetization (M_s) of 7.44 emu g^{-1}, which is lower than the reported M_s values for pristine hercynite (40 emu g^{-1}) and Hercynite@SiO_2 (28 emu g^{-1}).[18,21]

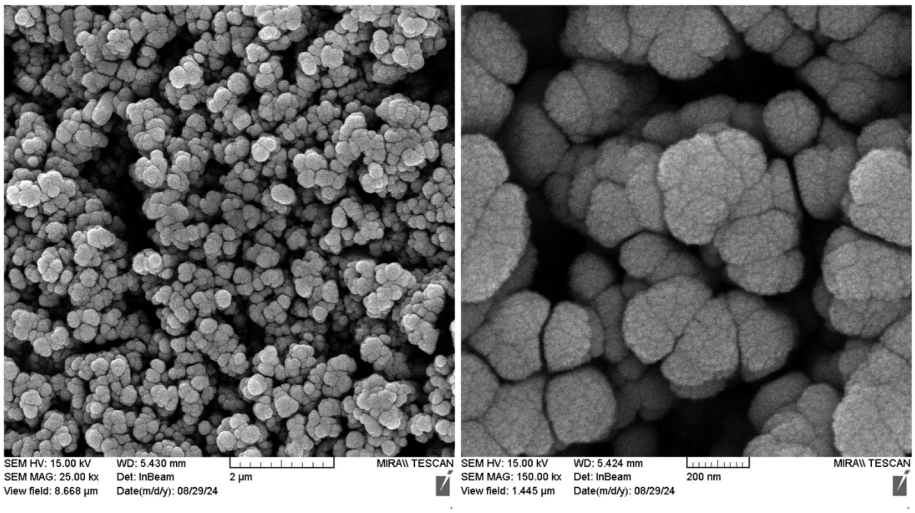

Fig. 6 SEM images of Hercynite@SiO_2-PMA.

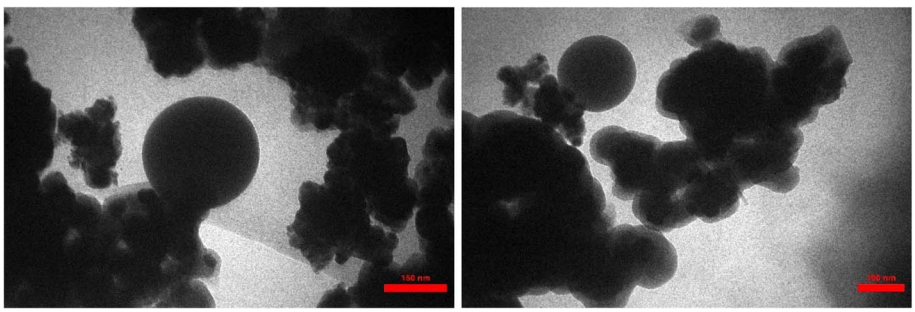

Fig. 7 TEM images of Hercynite@SiO_2-PMA.

This reduction is attributed to the presence of the diamagnetic SiO_2 and PMA groups, which dilute the overall magnetic response of the core material.[21,29] Although a neodymium magnet was employed to achieve rapid and efficient separation of the catalyst from the reaction medium, the Hercynite@SiO_2-PMA catalyst could also be effectively separated using a standard, ordinary magnet. This indicates that, despite its relatively low saturation magnetization, the catalyst maintains sufficient magnetic responsiveness for facile recovery with a simple external magnetic field. To illustrate this, a comparative image demonstrating the separation process using both a neodymium magnet and a conventional magnet is provided in the ESI (Fig. S1†).

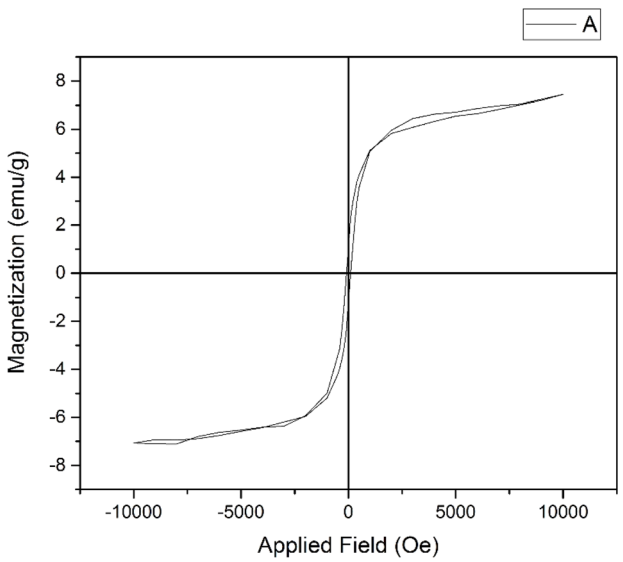

Fig. 8 VSM analysis of Hercynite@SiO_2-PMA.

The Hercynite@SiO_2-PMA possesses a moderate BET surface area of 12.07 $m^2\ g^{-1}$, indicating a sufficient capacity for adsorption (Fig. 9). It has a total pore volume of 0.04 $cm^3\ g^{-1}$ and an average pore diameter of 15.492 nm, indicating a relatively uniform pore size distribution. These attributes collectively render the catalyst highly suitable for diverse applications in heterogeneous catalysis.

3.2. Catalytic study

The catalytic activity of the Hercynite@SiO_2-PMA nanocomposite was evaluated in the synthesis of 2,3-dihydroquinazolin-4(1*H*)-ones *via* the cyclization of aldehyde or ketone compounds with 2-aminobenzamide under reflux

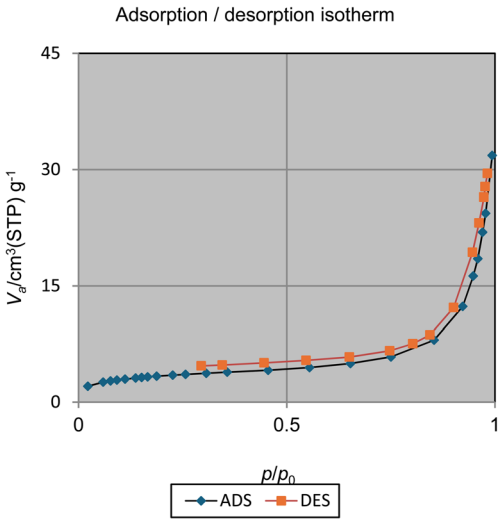

Fig. 9 N_2 adsorption/desorption isotherms of Hercynite@SiO_2-PMA.

condition. 4-Chlorobenzaldehyde was employed as a model substrate to optimize reaction conditions. A blank test confirmed the essential role of the catalyst in facilitating the reaction. In its absence, only trace amounts of the product were observed on TLC, even after an extended reaction time of 10 hours (Table 1, entry 1). When the Hercynite@SiO_2-PMA catalyst was introduced, the reaction commenced, and the product yield increased with increasing catalyst loading. Notably, a 20 mol% catalyst loading proved optimal, achieving complete conversion within 40 minutes. Further increasing the catalyst loading to 25 mol% did not significantly enhance the reaction kinetics or yield (Table 1, entry 6). Considering the environmental benefits of solvents, their impact on the reaction was explored. The reaction was also conducted in a mixed solvent system of water and ethanol. Although the results obtained from this mixed solvent were comparable to those achieved with pure water, water was ultimately selected as the optimal solvent due to its superior environmental friendliness (see Table 1, entries 5 and 7). In subsequent efforts to optimize the reaction conditions, the effect of temperature on yield and product formation rate was investigated. The reaction was conducted at room temperature using 20 mg of catalyst. however, as indicated in Table 1 (entry 8), only a negligible amount of product was obtained under these conditions. As a result, it was concluded that conducting the experiment at reflux temperature in water with 20 mg of catalyst was the optimal approach for achieving high yields and shorter reaction times.

The versatility of the optimized reaction conditions was investigated by reacting a range of aldehyde and ketone compounds with varying electronic properties. Fortunately, all reactions proceeded smoothly, yielding the desired products in high quantities. Sterically hindered aldehydes exhibited slower reaction rates compared to their less hindered counterparts. On the other hand, both types of carbonyl compounds—those containing electron-withdrawing groups (EWGs) and those with electron-donating groups (EDGs)—exhibited a notable rate enhancement, resulting in excellent yields. This broad substrate scope demonstrates the robustness and applicability of the developed method for a wide range of aldehyde and ketone compounds. Table 2 provides a comprehensive summary of the experimental procedures and the corresponding results.

The synthesis of 2,3-dihydroquinazolin-4(1*H*)-ones catalyzed by Hercynite@SiO_2-PMA nanocomposite proceeds *via* the pathway depicted in Scheme 2. Initially, the carbonyl group of the carbonyl compound is activated through coordination with the catalyst. This activation facilitates the nucleophilic attack of the amino nitrogen on the carbonyl carbon, leading to the

Table 1 Optimization of the 2,3-dihydroquinazolin-4(1*H*)-ones synthesis over the catalysis of Hercynite@SiO_2-PMA

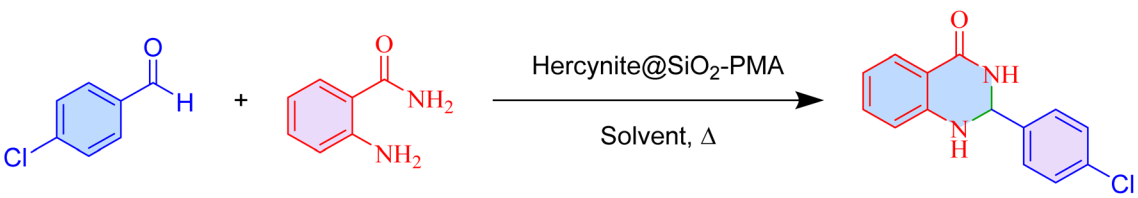

Entry	Amount of catalyst (mol%)	Solvent	Temperature (°C)	Time (min)	Yield[a,b] (%)
1	—	Water	Reflux	600	Trace
2	5	Water	Reflux	100	21
3	8	Water	Reflux	65	42
4	10	Water	Reflux	40	65
5	20	Water	Reflux	40	98
6	25	Water	Reflux	40	98
7	20	Ethanol/water	Reflux	60	98
8	20	Water	r.t	600	Trace

[a] Isolated yield. [b] Conditions: 2-aminobenzamide (1 mmol), 4-chlorobenzaldehyde (1 mmol), Hercynite@SiO_2-PMA catalyst (mg), and solvent (3 mL).

Table 2 Synthesis of 2,3-dihydroquinazolin-4(1*H*)-one derivatives over the catalysis of Hercynite@SiO_2-PMA nanocomposite

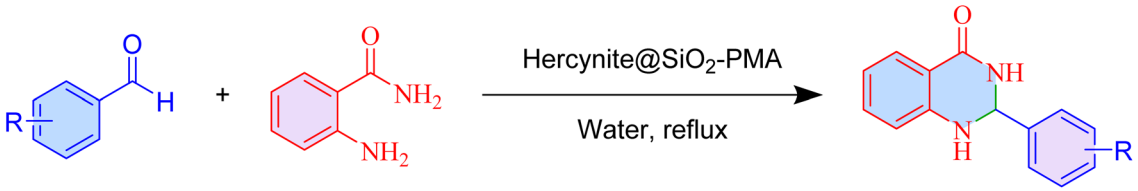

Entry	Carbonyl compound	Product	Time (min)	Yield[a,b] (%)	Melting point	
					Measured	Literature
1	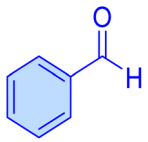	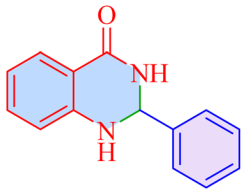	45	94	218–221	217–219 (ref. 12)
2	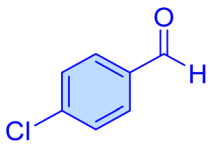	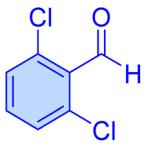	40	98	192–195	193–194 (ref. 7)
3	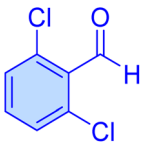	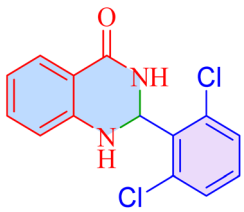	55	81	193–195	194–195 (ref. 38)
4	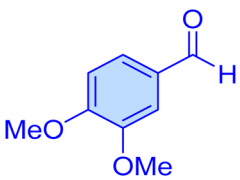	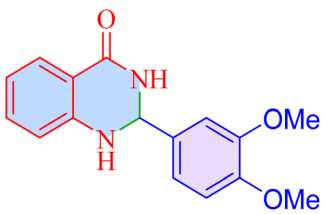	50	95	209–211	211–212 (ref. 7)
5	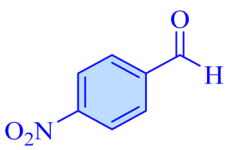	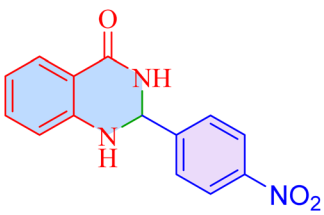	30	98	194–196	195–197 (ref. 7)
6	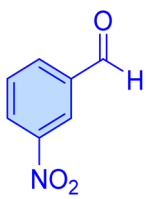	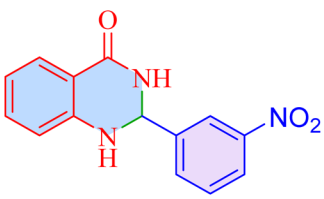	35	97	179–182	183–185 (ref. 39)
7	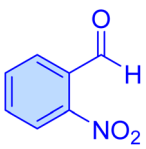	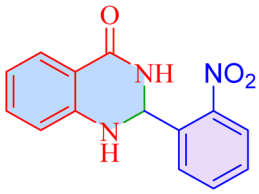	45	96	182–184	183–184 (ref. 39)

Table 2 (*Contd.*)

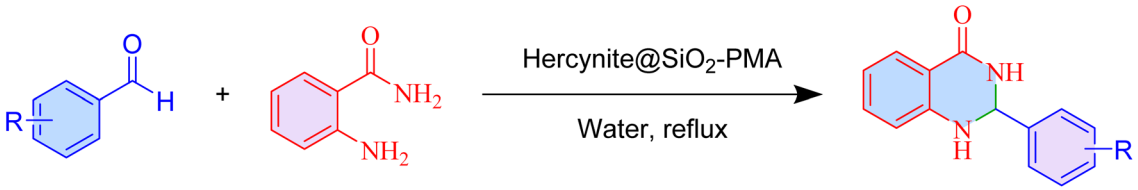

Entry	Carbonyl compound	Product	Time (min)	Yield[a,b] (%)	Melting point	
					Measured	Literature
8	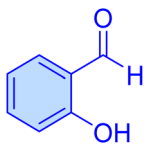	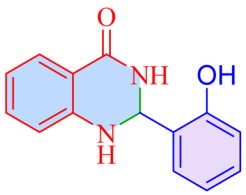	65	78	222–224	223–226 (ref. 40)
9	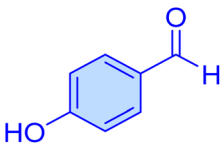	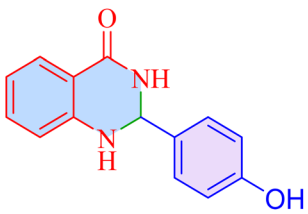	50	85	272–275	274–276 (ref. 7)
10	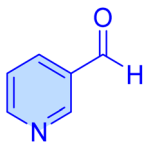	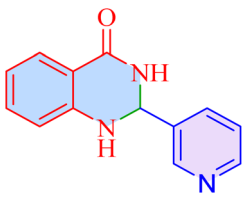	80	90	218–220	219–221 (ref. 41)
11	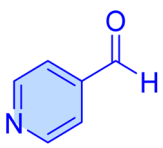	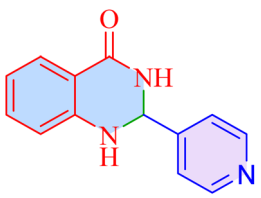	100	89	166–168	166–168 (ref. 42)
12	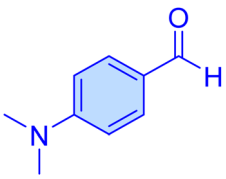	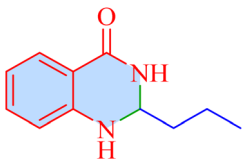	65	90	206–208	206–208 (ref. 43)
13	$CH_3CH_2CH_2CHO$	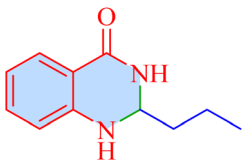	60	60	155–158	157–159 (ref. 44)
14	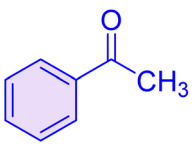	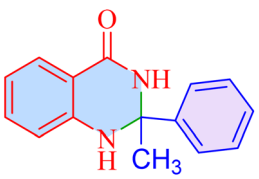	50	91	219–222	223–225 (ref. 45)

Table 2 (*Contd.*)

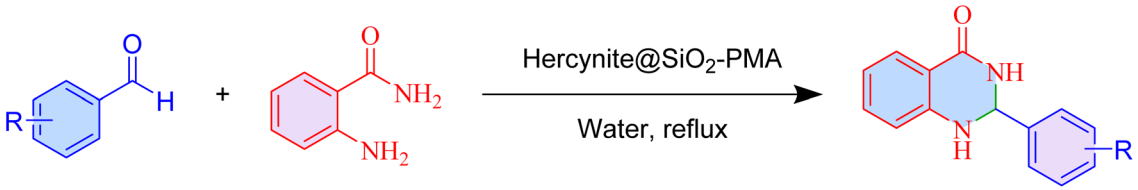

Entry	Carbonyl compound	Product	Time (min)	Yield[a,b] (%)	Melting point	
					Measured	Literature
15	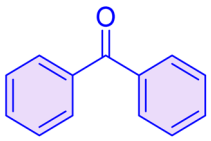	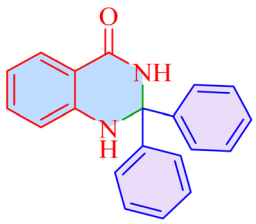	70	77	136–138	139–141 (ref. 45)

[a] Isolated yield. [b] Reaction conditions: aldehyde/ketone (1 mmol), anthranilamide (2-aminobenzamide) (1 mmol), Hercynite@SiO_2-PMA (20 mg), and water (3 mL) under reflux conditions.

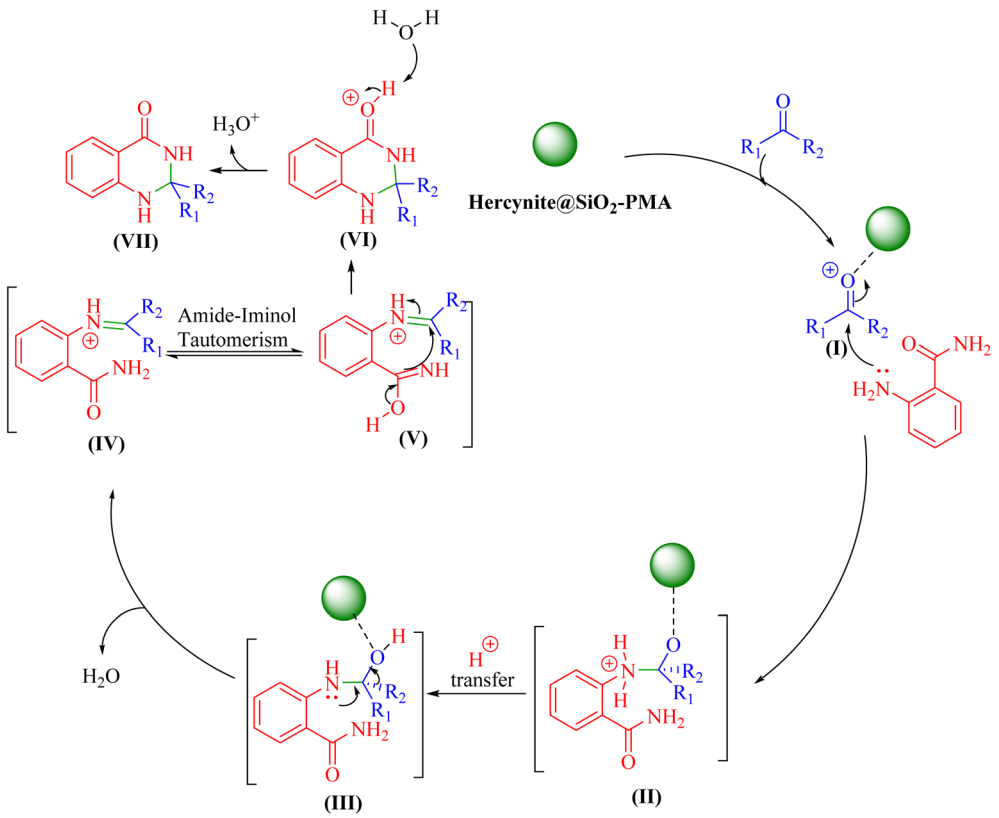

Scheme 2 Possible mechanism for the synthesis of 2,3-dihydroquinazolin-4(1*H*)-ones over the catalysis of Hercynite@SiO_2-PMA nanocomposite.

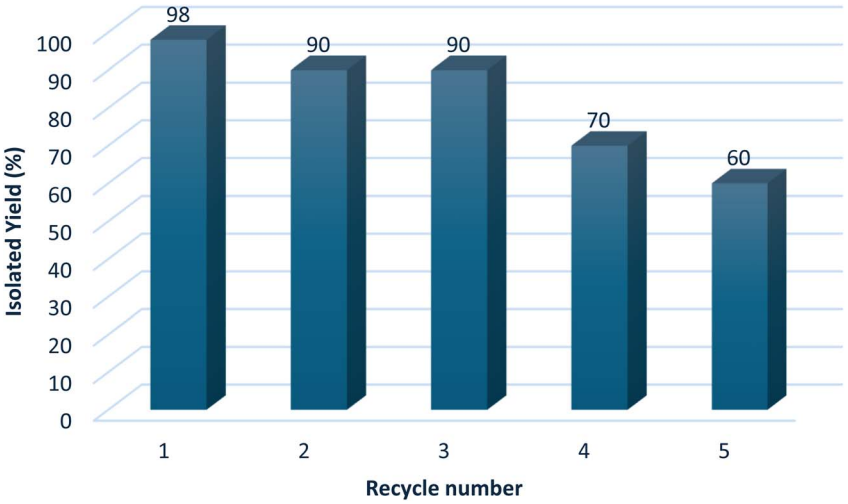

Fig. 10 The reusability of Hercynite@SiO_2-PMA nanocomposite.

formation of a tetrahedral intermediate. Subsequently, dehydration occurs, resulting in the formation of a Schiff base. The nucleophilic amide nitrogen then attacks the imine carbon, triggering ring closure and proton transfer, ultimately producing the desired 2,3-dihydroquinazolin-4(1*H*)-one.

3.3. Reusability of catalyst

The recyclability of the Hercynite@SiO_2-PMA nanocomposite was systematically evaluated over multiple catalytic cycles. Following each reaction, the catalyst was efficiently separated from the reaction mixture using magnetic separation. It was subsequently washed with hot ethanol and acetone to remove any residual reactants or products, then used in the next reaction cycle. The recovered catalyst exhibited excellent reusability in the initial runs. Although its efficiency declined after three cycles, it maintained good catalytic activity with minimal performance loss over five consecutive cycles (Fig. 10). To verify the structural stability of the catalyst, FT-IR spectrum of the recovered catalyst after five cycles was recorded. The spectrum indicates that the characteristic functional groups and overall structure of the catalyst are preserved, confirming its structural stability during the recycling process (ESI Fig. S18†). This consistent performance underscores the catalyst's durability, recyclability, and potential for cost-effective applications in catalytic processes.

Table 3 Comparison the efficiency of Hercynite@SiO_2-PMA nanocomposite in synthesis of 2,3-dihydroquinazolin-4(1*H*)-ones

Entry	Catalyst	Time (min)	Yield (%)	Reference
1	α-D-Glucose	180	61	46
2	SBA-16/GPTMS-TSC-Cu^I	35	95	47
3	$CoFe_2O_4$@Pr	60	97	7
4	Amberlyst-15	60	85	48
5	Lactic acid	30	90	49
6	Hercynite@SiO_2-PMA	40	98	This work

3.4. Comparison study of catalytic activity

A comparative analysis of the catalytic performance of the Hercynite@SiO_2-PMA nanocomposite was conducted with previously reported systems, focusing on reaction conditions and product yields (Table 3). While earlier studies often require longer reaction times, higher catalyst loadings, or expensive metal catalysts, the Hercynite@SiO_2-PMA reported here delivers comparable yields with benefits such as lower catalyst loadings, higher turnover frequencies, easy separation, and eco-friendly conditions.

4. Conclusions

In summary, this research describes the synthesis of nanomagnetic phosphomolybdic acid composite through surface functionalization of Hercynite-SiO_2 nanoparticles. This Hercynite@SiO_2-PMA nanocomposite has a unique structure enabling it to effectively catalyze the synthesis of 2,3-dihydroquinazolin-4(1*H*)-ones. The catalyst's performance is influenced by the steric and electronic properties of the aryl aldehyde starting materials. Importantly, the catalyst can be reused for up to three cycles without significant loss of activity, making it an environmentally friendly and efficient option for synthesizing N-heterocycles.

Data availability

The authors declare that all data in this manuscript are available upon request.

Author contributions

Kowsar Azizi: writing original draft, laboratory works, characterization of catalyst, software, and writing of manuscript Draft. Saba Ghasemi: supervision, conceptualization, analysis, review and edited the final version, and submitted manuscript for publication. Ahmad Nikseresht: providing key chemical

materials and instruments essential for the research, conceptualization, review and edited the final version.

Conflicts of interest

The authors declare that they have no competing interests.

Acknowledgements

This work was financially supported by Islamic Azad University of Ilam, Iran for which the authors are thankful. This research did not receive any specific grant from funding agencies in the public, commercial, or not-for-profit sectors.

References

1 M. Badolato, F. Aiello and N. Neamati, *RSC Adv.*, 2018, **8**, 20894–20921.
2 M. Bhat, S. L. Belagali, S. V. Mamatha, B. K. Sagar and E. V. Sekhar, *Stud. Nat. Prod. Chem.*, 2021, **71**, 185–219.
3 M. Faheem, A. K. Tiwari and V. K. Singh, *Curr. Org. Chem.*, 2020, **24**, 1108–1138.
4 O. Babatunde, S. Hameed, U. Salar, S. Chigurupati, A. Wadood, A. U. Rehman, V. Venugopal, K. M. Khan, M. Taha and S. Perveen, *Mol. Divers.*, 2022, **26**, 849–868.
5 M. Mohammadi and A. Ghorbani-Choghamarani, *RSC Adv.*, 2022, **12**, 2770–2787.
6 J. Mou, N. Chen, Y. Zhao, H. Qi, S. Meng, R. Xiang and D. Pei, *Front. Chem.*, 2020, **8**, 239.
7 A. Ghorbani-Choghamarani, H. Aghavandi and M. Mohammadi, *J. Porous Mater.*, 2021, **28**, 1167–1186.
8 P. Munnik, P. E. de Jongh and K. P. de Jong, *Chem. Rev.*, 2015, **115**, 6687–6718.
9 M. Mohammadi, M. Khodamorady, B. Tahmasbi, K. Bahrami and A. Ghorbani-Choghamarani, *J. Ind. Eng. Chem.*, 2021, **97**, 1–78.
10 Q. Sun, N. Wang and J. Yu, *Adv. Mater.*, 2021, **33**, 2104442.
11 R. Schlögl, *Angew. Chem., Int. Ed.*, 2015, **54**, 3465–3520.
12 M. A. K. Zarchi, F. Hajati and B. F. Mirjalili, *J. Polym. Res.*, 2022, **29**, 252.
13 Y. Zou, Z. Sun, Q. Wang, Y. Ju, N. Sun, Q. Yue, Y. Deng, S. Liu, S. Yang, Z. Wang, F. Li, Y. Hou, C. Deng, D. Ling and Y. Deng, *Chem. Rev.*, 2025, **125**, 972–1048.
14 Q. Zhang, X. Yang, J. Guan and A. C. S. Appl, *Nano Mater.*, 2019, **2**, 4681–4697.
15 D. Wang and D. Astruc, *Chem. Rev.*, 2014, **114**, 6949–6985.
16 S. Walake, R. Gumathannawar, S. Mane, R. Shendkar, A. Rokade, M. Shirolkar and Y. Jadhav, *J. Exp. Nanosci.*, 2024, **19**, 2416113.
17 M. Mohammadi and A. Ghorbani-Choghamarani, *New J. Chem.*, 2020, **44**, 2919–2929.
18 A. Ghorbani-Choghamarani, M. Mohammadi, L. Shiri and Z. Taherinia, *Res. Chem. Intermed.*, 2019, **45**, 5705–5723.
19 M. Daghetta, M. Dapiaggi, L. Pellegrino, B. Pastore, L. Pagliari and C. Mazzocchia, *Chem. Eng. Trans.*, 2015, **43**, 1741–1746.
20 S. Beiranvand, M. Norouzi and B. Tahmasbi, *Curr. Org. Chem.*, 2024, **28**, 777–788.
21 M. Mohammadi and A. Ghorbani-Choghamarani, *RSC Adv.*, 2022, **12**, 26023–26041.
22 M. Mohammadi and G. Mansouri, *Langmuir*, 2024, **40**, 22773–22786.
23 Hartati, P. B. D. Firda, H. Bahruji and M. B. Bakar, *Flavour Fragrance J.*, 2021, **36**, 509–525.
24 A. Nikseresht, R. Bagherinia, M. Mohammadi and R. Mehravar, *RSC Adv.*, 2023, **13**, 674–687.
25 S. Takale, S. Manave, K. Phatangare, V. Padalkar, N. Darvatkar and A. Chaskar, *Synth. Commun.*, 2012, **42**, 2375–2381.
26 E. Rafiee, H. Mahdavi and M. Joshaghani, *Mol. Divers.*, 2011, **15**, 125–134.
27 Á. Molnár, C. Keresszegi and B. Török, *Appl. Catal., A*, 1999, **189**, 217–224.
28 J. Xue and C. Liu, *Asian J. Chem.*, 2008, **20**, 4859–4865.
29 A. Nikseresht, M. Karami and M. Mohammadi, *Langmuir*, 2024, **40**, 18512–18524.
30 M. Mohammadi and A. Ghorbani-Choghamarani, *Appl. Organomet. Chem.*, 2022, **36**, e6905.
31 M. Ghasemirad, M. Norouzi and P. Moradi, *J. Nanoparticle Res.*, 2024, **26**, 14.
32 S. Beheshti, A. Motavalizadehkakhky, R. Zhiani, S. M. M. Nouri and E. Zahedi, *Sci. Rep.*, 2024, **14**, 11969.
33 N. Zabeti, A. K. Keyhanizadeh, A. R. Faraji, M. Soltani, S. Saeedi, E. Tehrani and Z. Hekmatian, *Int. J. Biol. Macromol.*, 2024, **254**, 127897.
34 E. J. W. Verwey and E. L. Heilmann, *J. Chem. Phys.*, 1947, **15**, 174–180.
35 L. Lian, S. Zhang, N. Ma and W. Dai, *Polyhedron*, 2021, **207**, 115402.
36 M. Taghavi, M. Tabatabaee, M. H. Ehrampoush, M. T. Ghaneian, M. Afsharnia, A. Alami and J. Mardaneh, *J. Mol. Liq.*, 2018, **249**, 546–553.
37 N. C. Coronel and M. J. da Silva, *J. Cluster Sci.*, 2018, **29**, 195–205.
38 J. Devi, S. J. Kalita and D. C. Deka, *Synth. Commun.*, 2017, **47**, 1601–1609.
39 H. R. Safaei, M. Shekouhy and S. Ghorbanzadeh, *ChemistrySelect*, 2018, **3**, 4750–4759.
40 M. Beyki and M. Fallah-Mehrjardi, *Lett. Org. Chem.*, 2017, **15**, 39–44.
41 B. Mitra, G. Chandra Pariyar and P. Ghosh, *RSC Adv.*, 2021, **11**, 1271–1281.
42 N. Azizi, F. Abbasi and M. Abdoli-Senejani, *Mater. Chem. Phys.*, 2017, **196**, 118–125.
43 G. K. Kharmawlong, R. Nongrum, B. Chhetri, J. W. S. Rani, N. Rahman, A. K. Yadav and R. Nongkhlaw, *Synth. Commun.*, 2019, **49**, 2683–2695.

44 A. Ghorbani-Choghamarani and M. Norouzi, *J. Mol. Catal. A Chem.*, 2014, **395**, 172–179.
45 S. Das, S. Santra, S. Jana, G. V. Zyryanov, A. Majee and A. Hajra, *Eur. J. Org Chem.*, 2017, **2017**, 4955–4962.
46 T. dos Santos, C. Grundke, T. Lucas, L. Großmann, G. C. Clososki and T. Opatz, *Eur. J. Org. Chem.*, 2020, **2020**, 6429–6432.
47 M. A. Erfan, B. Akhlaghinia and S. S. E. Ghodsinia, *ChemistrySelect*, 2020, **5**, 2306–2316.
48 S. B. Bharate, N. Mupparapu, S. Manda, J. B. Bharate, R. Mudududdla, R. R. Yadav and R. A. Vishwakarma, *Arkivoc*, 2012, **2012**, 308–318.
49 S. Zhaleh, N. Hazeri and M. T. Maghsoodlou, *Res. Chem. Intermed.*, 2016, **42**, 6381–6390.